

Fermi National Accelerator Laboratory

FERMILAB-Conf-99/280-E

E835

**Measurements of the Magnetic Form Factor of the Proton at Large
Timelike Momentum Transfers**

Giulio Stancari
For the E835 Collaboration

*Fermi National Accelerator Laboratory
P.O. Box 500, Batavia, Illinois 60510*

October 1999

Published Proceedings of the *Second International Conference on Perspectives in Hadronic Physics, I.C.T.P.*, Trieste, Italy, May 10-14, 1999

Disclaimer

This report was prepared as an account of work sponsored by an agency of the United States Government. Neither the United States Government nor any agency thereof, nor any of their employees, makes any warranty, expressed or implied, or assumes any legal liability or responsibility for the accuracy, completeness, or usefulness of any information, apparatus, product, or process disclosed, or represents that its use would not infringe privately owned rights. Reference herein to any specific commercial product, process, or service by trade name, trademark, manufacturer, or otherwise, does not necessarily constitute or imply its endorsement, recommendation, or favoring by the United States Government or any agency thereof. The views and opinions of authors expressed herein do not necessarily state or reflect those of the United States Government or any agency thereof.

Distribution

Approved for public release; further dissemination unlimited.

Copyright Notification

This manuscript has been authored by Universities Research Association, Inc. under contract No. DE-AC02-76CH03000 with the U.S. Department of Energy. The United States Government and the publisher, by accepting the article for publication, acknowledges that the United States Government retains a nonexclusive, paid-up, irrevocable, worldwide license to publish or reproduce the published form of this manuscript, or allow others to do so, for United States Government Purposes.

MEASUREMENTS OF THE MAGNETIC FORM FACTOR OF THE PROTON AT LARGE TIMELIKE MOMENTUM TRANSFERS

GIULIO STANCARI

*Antiproton Source Department and E-835 Collaboration
Fermi National Accelerator Laboratory, Batavia, IL 60510, USA
E-mail: stancari@fnal.gov*

Results obtained by Fermilab experiment E-835 during its 1996–1997 data-taking run are presented. In this experiment, the magnetic form factor of the proton is measured by observing the reaction $\bar{p}p \rightarrow e^+e^-$ in the center-of-momentum energy interval between 2.9 GeV and 4.3 GeV, corresponding to q^2 between $8.8 (\text{GeV}/c)^2$ and $18.4 (\text{GeV}/c)^2$. The stochastically-cooled circulating antiproton beam intersects an internal hydrogen gas jet target; the e^+e^- final states are identified by a non-magnetic spectrometer. In spite of the smallness of the reaction cross section compared to the hadronic background, a total of 144 signal events is observed, yielding the most precise high-energy results to date.

1 Introduction

Within the framework of Quantum Electrodynamics, the electromagnetic properties of the proton are parameterized by two quantities, the electric and magnetic form factors $G_E(q^2)$ and $G_M(q^2)$, which are functions of the squared four-momentum transfer q^2 .^{1–5}

In the spacelike region ($q^2 < 0$), the electric and magnetic form factors have been measured with high precision in elastic electron-proton scattering up to $|q^2| = 10 (\text{GeV}/c)^2$ and $|q^2| = 31 (\text{GeV}/c)^2$, respectively.^{6–9} Measurements for timelike momentum transfers ($q^2 = s > 0$) come from the reactions $e^+e^- \rightarrow p\bar{p}$ and $\bar{p}p \rightarrow e^+e^-$.^{10–18} They are mostly concentrated in an interval near threshold: $4m_p^2 \leq s \leq 7 \text{ GeV}^2$ (m_p is the proton's rest energy). One of the main reasons is that G_E and G_M are rapidly decreasing functions of q^2 , making cross sections hardly accessible as q^2 increases. The first attempt to make measurements at larger momentum transfer was made by CERN experiment R-704, but only upper limits were established at $s = 8.9 \text{ GeV}^2$ and 12.5 GeV^2 .¹⁹ The first non-zero measurements were reported by Fermilab experiment E-760, which obtained $|G_M|$ at $s = 8.9, 12.4$ and 13.0 GeV^2 .²⁰ In this paper, new improved measurements of the proton's magnetic form factor are presented,^a for momentum transfers up to $q^2 = 14.4 \text{ GeV}^2$.

^a A paper on the same subject by the E-835 collaboration (M. Ambrogiani *et al.*), containing

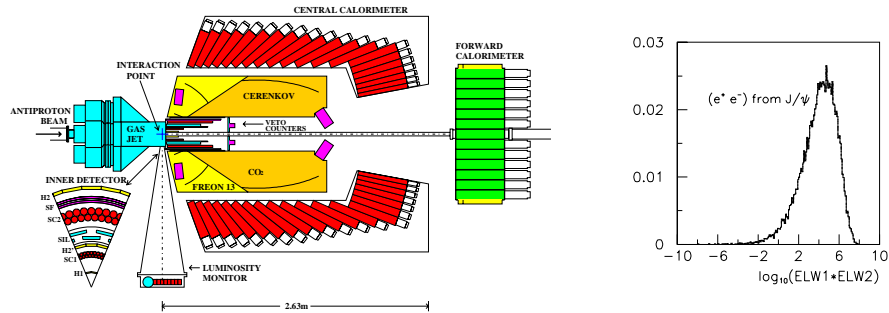


Figure 1. (left) E-835 experimental layout. (right) Distribution of the product of ELW indices for electrons from a clean sample of $J/\psi \rightarrow e^+ e^-$ decays.

The antiproton-proton annihilation into an electron-positron pair $\bar{p}p \rightarrow e^+ e^-$ has been studied in the center-of-momentum (c.m.) energy interval between 2.9 GeV and 4.3 GeV. The differential cross section can be expressed in terms of the proton's electric and magnetic form factors as follows:²¹

$$\frac{d\sigma}{d(\cos\theta^*)} = \frac{\pi\alpha^2\hbar^2c}{8EP} \left[|G_M|^2 (1 + \cos^2\theta^*) + \frac{4m_p^2}{s} |G_E|^2 \sin^2\theta^* \right],$$

where, in the c.m. frame, E and P are the energy and momentum of the antiproton, and θ^* is the angle between the electron and the antiproton momenta.

2 Experimental Apparatus

Experiment E-835 is dedicated to the study of charmonium by resonant formation in $\bar{p}p$ annihilations. It was carried out at the Fermilab Antiproton Accumulator and took data from October 1996 through September 1997, collecting a total integrated luminosity of 143 pb^{-1} . The charmonium physics program determined the choices of c.m. energy and of integrated luminosity accumulated in each energy region.^b

Some of the experimental requirements for charmonium physics make this experiment an excellent place for the study of timelike form factors. The high-quality antiproton beam, the variable-density hydrogen gas jet target, and the

^amore details on this analysis, will appear in the August 1, 1999 issue of Physical Review D.

^bFor more information, the reader can refer to the experiment's web site: <http://www-e835.fnal.gov>.

powerful e^+e^- tagging system (which are described below) make it possible to reach high luminosities and, at the same time, to suppress the otherwise huge background arising from the $\bar{p}p$ total cross section.

As shown schematically in Figure 1 (left), the circulating beam of stochastically-cooled antiprotons (up to 5×10^{11} particles) intersects the internal hydrogen gas jet target.²² During the data-taking run, as the beam current decreases, the target density is increased so as to keep the instantaneous luminosity constant, around $2 \times 10^{31} \text{ cm}^{-2} \text{ s}^{-1}$. This value is close to the maximum rate that the detector and the data-acquisition system can efficiently handle; therefore, the integrated luminosity collected is maximized. The measurement of the luminosity is provided by three silicon detectors positioned at $\theta = 86.5^\circ$ to the \bar{p} beam direction, monitoring the yield of elastic recoil protons;²³ the uncertainty is less than $\pm 2.5\%$. The interaction region, as determined by the intersection of the beam with the gas jet, is approximately $(5 \times 5 \times 7) \text{ mm}^3$. By measuring the revolution frequency of the beam (through a Schottky-noise spectrum) and its orbit length (with beam-position monitors), the beam energy was determined with an uncertainty between 0.2 MeV and 2.0 MeV.

The E-835 apparatus (Figure 1, left) has been designed to detect electromagnetic final states. It makes use of some of the components employed in experiment E-760,²⁰ as well as several upgrades. It is a non-magnetic spectrometer with full azimuthal (ϕ) coverage and polar angle (θ) acceptance ranging from 2° to 70° . The central detector ($11^\circ < \theta < 70^\circ$) has cylindrical symmetry around the beam axis; its main components are the lead-glass electromagnetic calorimeter, the threshold gas Cherenkov counter for e^\pm/π discrimination and the inner tracking system.

The central calorimeter (CCAL)²⁴ is a matrix of 1280 lead-glass counters (64 in ϕ by 20 in θ) pointing to the interaction region, measuring the energy and direction of electrons, positrons and photons. It has an energy resolution $\sigma_E/E = 0.014 + 0.06/\sqrt{E(\text{GeV})}$ and an angular resolution (r.m.s.) of 11 mrad in ϕ and 6 mrad in θ (these angular errors include the contribution due to the finite size of the interaction region). Each counter is equipped with a time-to-digital converter (TDC), which provides timing information to reject pile-up. All showers with energy above 80 MeV can be identified as ‘in-time’ or ‘out-of-time’. Showers with lower energy sometimes have no TDC information and are then labeled ‘undetermined’.

The Cherenkov counter²⁵ contains 16 cells (8 in ϕ by 2 in θ); it covers the full azimuth and from 15° to 65° in θ . The counter is a threshold device and serves to identify electrons and to reject pions at the trigger level, and to distinguish single electrons from e^+e^- pairs in the off-line analysis.

The inner tracking system consists of two layers of straw-tube drift cham-

bers (SC1 and SC2) ²⁶ for the measurement of ϕ and a scintillating fiber tracker (SF) with VLPC readout ²⁷ for the measurement of θ . The angular resolution is 11 mrad in ϕ , whereas in θ it varies from 3 mrad at small angles to 11 mrad at large angles. The intrinsic resolution of the scintillating fiber detector is better than 2 mrad, but the θ resolution is dominated by the size of the interaction region.

Three cylindrical plastic scintillator hodoscopes (H1, H2' and H2) located at increasing distances from the beam axis are used for triggering. The pulse heights, together with those in the Cherenkov counter, are used off-line to distinguish singly charged particles from e^+e^- pairs due to photon conversions and to π^0 Dalitz decays.

The polar angle region from 2° to 12° is covered by a planar forward calorimeter and by a plastic scintillator hodoscope, not used in this analysis.

The experiment uses the DART data-acquisition system to acquire and store data. ²⁸ At a typical luminosity, the first-level trigger rate is 1 KHz and the live-time is greater than 90%.

3 Event Selection

In this analysis, signal cross sections of a few picobarns must be measured in presence of a ≈ 60 mb total cross section, i.e. a rejection factor of the order of 10^{10} must be achieved. The selection of $\bar{p}p \rightarrow e^+e^-$ is essentially based upon identification of electrons and positrons and on kinematics.

3.1 Selection Criteria

The first-level trigger for e^+e^- events requires two 'electron tracks', each defined by a coincidence between the appropriate azimuthal elements of H1, H2 and the corresponding cells of the Cherenkov counter;^c independently, two high-energy showers are required in the central calorimeter, with an azimuthal opening angle greater than 90° .

Events which satisfy the hardware trigger are processed by the on-line filter, which selects those in which the two highest-energy clusters in the CCAL have an invariant mass greater than $2 \text{ GeV}/c^2$.

Electron tracks are reconstructed off-line by associating hodoscope hits, Cherenkov counter signals and calorimeter showers. Track information from the inner detectors is added to improve the angular resolution. The two electron candidates are identified as the tracks with the highest invariant

^cObviously, the detector cannot distinguish between electrons and positrons.

mass. The selection of $\bar{p}p \rightarrow e^+e^-$ proceeds in four steps.

(a) *Electron identification.* For each candidate electron track, an electron weight index (ELW) is constructed using the pulse heights in the H1, H2, H2' and Cherenkov counters, second moments of the transverse shower distribution in CCAL and the fractional shower energy in a 3×3 block region of CCAL. ELW is a likelihood ratio for the electron hypothesis versus the background hypothesis. Since in a good event both candidates are required to be good electron tracks, the product of the ELW indices of the two candidate electrons is used. The distribution of $\log_{10}(\text{ELW}_1 \cdot \text{ELW}_2)$ in a clean electron sample is shown in Figure 1 (right). In order to reduce the size of the data sample, a preliminary selection is applied to the raw data by imposing a loose cut on the product of the ELW for the two electron candidates ($\text{ELW}_1 \times \text{ELW}_2 > 0.1$): only events which pass this preliminary selection undergo the subsequent analysis. In the final selection, the electron weight cut is $\text{ELW}_1 \times \text{ELW}_2 > 1$.

(b) *Fiducial volume.* The cut in fiducial volume is necessary in order to remove inhomogeneities in the response of the detector at its edges. For this reason we accept only events in which the two electron candidates have polar angles in the interval $15^\circ < \theta < 60^\circ$, well within the angular coverage of CCAL and of the Cherenkov counter.

(c) *CCAL multiplicity.* To avoid rejecting events in which the electron or positron radiates a Bremsstrahlung photon which forms a distinct cluster in the CCAL, we do not impose a strict cut demanding only two in-time clusters. Events with more than two in-time clusters are kept provided that the extra clusters, when paired with either electron candidate, give an invariant mass below $100 \text{ MeV}/c^2$. In addition, any number of out-of-time or undetermined clusters is allowed.

(d) *Kinematic fit.* The goodness of the two body hypothesis is finally tested by means of a four-constraint kinematic fit. All candidate events are tested with this hypothesis and are accepted if the fit probability is above 1%.

The number N of events selected with these criteria is shown in Table 1 for each energy region.

3.2 Efficiency

The overall efficiency ε is the product of the trigger efficiency ε_{tri} and the efficiencies of the preliminary selection ε_{pre} and of the off-line analysis ε_{ana} : $\varepsilon = \varepsilon_{\text{tri}} \cdot \varepsilon_{\text{pre}} \cdot \varepsilon_{\text{ana}}$.

The trigger efficiency ε_{tri} has been measured with a special trigger run at the J/ψ energy, which required only one electron track in the H1, H2 and

Cherenkov counters, in addition to the two-cluster requirement in the central calorimeter; the result is $\varepsilon_{\text{tri}} = 0.898 \pm 0.005$.

The efficiency of the preliminary off-line cut $\text{ELW}_1 \times \text{ELW}_2 > 0.1$ has been measured using clean samples of $J/\psi \rightarrow e^+e^-$ and $\psi' \rightarrow e^+e^-$ events selected by means of topological cuts and a kinematical fit and has been found to be $\varepsilon_{\text{pre}} = 0.966 \pm 0.001$.

The efficiency of the second set of off-line cuts has been evaluated at the J/ψ and ψ' energies. Background contamination is estimated with data taken off resonance and rescaled by luminosity. The efficiency of the off-line analysis is found to be 0.777 ± 0.004 at the J/ψ and 0.75 ± 0.01 at the ψ' . A single value of $\varepsilon_{\text{ana}} = 0.764 \pm 0.003(\text{stat}) \pm 0.045(\text{syst})$ is assumed, where the systematic error takes into account the difference in efficiency found at the J/ψ and at the ψ' , the variation of efficiency with time and the effect of the background subtraction procedure.

The overall efficiency used at all energies is thus $\varepsilon = 0.663 \pm 0.005(\text{stat}) \pm 0.05(\text{syst})$.

3.3 Background Contamination

Because of the smallness of the signal cross section compared to the total cross section, a careful analysis of possible background processes has been performed. In the E-835 detector, the main sources of background for the reaction $\bar{p}p \rightarrow e^+e^-$ are the following: (a) processes with production of π^0 s, because of photon conversions and Dalitz decays); (b) two-body hadronic final states, mainly $\pi^+\pi^-$ and K^+K^- , when a δ -ray fires the Cherenkov cells and a hadron shower is generated in the CCAL with energy and shape similar to an e.m. shower; (c) inclusive $J/\psi X$ events, if the undetected system X carries little momentum and the J/ψ decays into an e^+e^- pair.

Conservative estimates give an expected total background of 9.0×10^{-2} pb at 2.9 GeV and 2.9×10^{-2} pb at 3.5 GeV, corresponding to approximately one event at both energies. Therefore, no subtraction from the number of candidate events is performed.

4 Results

The number N of events collected with an integrated luminosity L and an overall efficiency ε is

$$N = \varepsilon L \sigma_{\text{acc}},$$

Table 1. Summary of the results of the form factor analysis. For each energy region, the integrated luminosity L , the number of selected events N , the cross section $\sigma_{\text{acc}} \equiv N/(L \varepsilon)$ and the geometrical acceptance in the c.m. frame are shown. The results correspond to the two hypotheses described in the text: (a) $G_E = G_M$ and (b) negligible ‘electric’ contribution. An upper limit at the 90% confidence level is reported where there are no observed events. The errors shown are statistical and systematic, respectively. The systematic uncertainty is due to the errors on efficiency and luminosity. The error on s , due to the grouping of several runs at different energies, is also included in the systematic error. The various contributions to the systematic errors are added linearly.

s (GeV ²)	L (pb ⁻¹)	N	σ_{acc} (pb)	$ \cos \theta^* _{\text{max}}$	$10^2 \times G_M $	
					(a)	(b)
8.84 ± 0.16	17.69	93	$7.93^{+0.82+1.00}_{-0.82-0.69}$	0.451	$3.59^{+0.18+0.23}_{-0.19-0.17}$	$4.17^{+0.21+0.26}_{-0.22-0.19}$
10.78 ± 0.28	1.78	3	$2.5^{+1.9+0.3}_{-1.6-0.2}$	0.544	$2.13^{+0.70+0.15}_{-0.84-0.11}$	$2.40^{+0.79+0.15}_{-0.95-0.12}$
12.43 ± 0.02	47.84	33	$1.04^{+0.18+0.13}_{-0.18-0.09}$	0.601	$1.43^{+0.12+0.09}_{-0.13-0.07}$	$1.58^{+0.13+0.10}_{-0.14-0.07}$
13.11 ± 0.18	33.99	14	$0.62^{+0.19+0.08}_{-0.16-0.05}$	0.621	$1.12^{+0.16+0.07}_{-0.16-0.06}$	$1.24^{+0.18+0.08}_{-0.18-0.06}$
14.36 ± 0.50	1.86	1	$0.8^{+1.4+0.1}_{-0.5-0.1}$	0.604	$1.39^{+0.91+0.13}_{-0.54-0.11}$	$1.51^{+1.00+0.14}_{-0.59-0.12}$
18.40 ± 0.01	0.76	0	< 4.88	0.508	< 4.40	< 4.74

where the term σ_{acc} is the differential cross section integrated over the c.m. acceptance region:

$$\begin{aligned} \sigma_{\text{acc}} &\equiv \int_{-|\cos \theta^*|_{\text{max}}}^{+|\cos \theta^*|_{\text{max}}} \left[\frac{d\sigma}{d(\cos \theta^*)} \right] d(\cos \theta^*) \\ &= \frac{\pi \alpha^2 \hbar^2 c}{8EP} \cdot \left[A \cdot |G_M|^2 + \frac{4m_p^2}{s} \cdot B \cdot |G_E|^2 \right]. \end{aligned}$$

At different values of s , the fiducial range $15^\circ < \theta < 60^\circ$ used in the event selection corresponds to different acceptances for θ^* . At $\sqrt{s} < 3.661$ GeV, it is the upstream edge of the fiducial range ($\theta = 60^\circ$) that determines $|\cos \theta^*|_{\text{max}}$; whereas for $\sqrt{s} > 3.661$ GeV it is the downstream edge ($\theta = 15^\circ$) that constrains the acceptance. The fact that the E-835 apparatus cannot distinguish between electrons and positrons is taken into account by integrating from $-|\cos \theta^*|_{\text{max}}$ to $+|\cos \theta^*|_{\text{max}}$. The acceptance coefficients A and B are:

$$A \equiv 2 \cdot \int_0^{|\cos \theta^*|_{\text{max}}} (1 + \cos^2 \theta^*) d(\cos \theta^*)$$

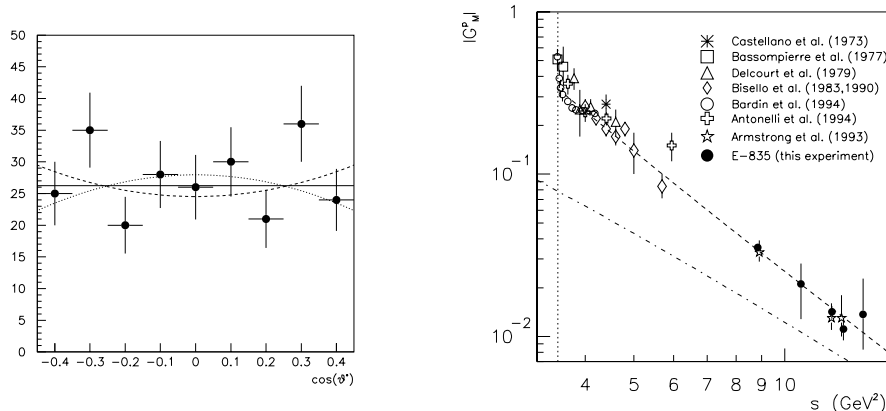


Figure 2. (Left) Angular distribution of all events in the c.m. acceptance region common to all energy points (two entries per event). Functional forms corresponding to different hypotheses ($|G_E| = 0$, $|G_M| = 0$ and isotropic) are equally compatible with the data ($\chi^2 = 0.8$). (Right) All existing measurements of the magnetic form factor of the proton, including the results of this experiment (\bullet). All values correspond to the $G_E = G_M$ hypothesis. A few upper limit values quoted in the references have been omitted for clarity. The dashed and dot-dashed curves are explained in the text.

$$B \equiv 2 \cdot \int_0^{|\cos \theta^*|_{\max}} (1 - \cos^2 \theta^*) d(\cos \theta^*).$$

For small $|\cos \theta^*|_{\max}$, A is approximately equal to B , and the relative importance of the ‘electric’ and ‘magnetic’ contributions is weighted by $4m_p^2/s$ only. As $|\cos \theta^*|_{\max}$ approaches one, the ratio A/B tends to 2, and the ‘electric’ contribution is further suppressed. Since the small number of events and the limited $\cos \theta^*$ range do not allow us to measure the angular distribution (Figure 2, left), two alternative hypotheses are made: (a) $G_E = G_M$, as is the case at the threshold of the timelike region ($s = 4m_p^2$); (b) the ‘electric’ contribution is assumed to be negligible. Under hypothesis (b), the measurement of the magnetic form factor of the proton is achieved through the following relation:

$$|G_M| = \frac{1}{\alpha \hbar} \cdot \sqrt{\frac{8}{\pi c}} \cdot \left[\frac{E P N}{\varepsilon A L} \right]^{\frac{1}{2}}.$$

Under hypothesis (a), A is replaced by $A + (4m_p^2/s) \cdot B$. The results obtained are shown in Table 1. It should be observed that the values of $|G_M|$ determined in the two hypotheses differ by less than 15%. The values of $|G_M|$

obtained under assumption (a) are plotted in Figure 2, where they are compared with E-760 results and with earlier measurements. The magnitude of the observed cross sections σ_{acc} relative to the total $\bar{p}p$ cross section (≈ 70 mb) should be emphasized. Some data have been taken above the ψ' resonance at $s = 18.4$ GeV². Since no e^+e^- events have been observed, an upper limit on the form factor is given in Table 1, corresponding to a 90% confidence level.²⁹

Figure 2 shows a fit to the data in the form

$$|G_M| = \frac{C}{s^2 \ln^2(s/\Lambda^2)} \quad (1)$$

where $\Lambda = 0.3$ GeV is the QCD scale parameter and C is a free parameter (dashed line). This functional form comes from the perturbative-QCD prediction^{30,31} that, for large momentum transfers, $q^4 G_M$ should be nearly proportional to the square of the running coupling constant for strong interactions $\alpha_s^2(q^2)$. The dipole behavior of the form factors in the spacelike region for the same values of $|q^2|$ is also plotted in Figure 2 (dot-dashed line). The fit can reproduce the data very well ($\chi^2 = 0.3$), even though the asymptotic regime has not been reached. In fact, there is still an appreciable difference between the timelike and spacelike form factors. In Figure 2, the spacelike form factor at $-q^2$ is represented by the dipole functional form (dot-dashed line); the timelike form factor appears to be 1.5 to 3 times larger, depending upon the energy. This is consistent with the findings of E-760²⁰ and with calculations based on the quark-diquark model of the proton.³² A similar result has been obtained from rigorous QCD calculations on the form factors of mesons.³³

5 Conclusion

The concurrence of the goals of charmonium and form-factor physics has brought about a breakthrough in the study of the proton's structure. The most recent of the experimental projects pursuing both of these research objectives is Fermilab E-835, whose form-factor results are discussed in this paper. A new data-taking run is foreseen starting from the winter of 1999.

Acknowledgements

The author wishes to thank the organizers of the conference for the invitation to participate and for providing such a stimulating and enjoyable environment. He also gratefully acknowledges the contributions and support of the Fermi-

lab Particle Physics Division, the Fermilab Beams Division and the E-835 collaborators.

This research was funded in part by the U.S. Department of Energy and by the Italian Istituto Nazionale di Fisica Nucleare.

References

1. M.N. Rosenbluth, *Phys. Rev.* **79**, 615 (1950).
2. L.L. Foldy, *Phys. Rev.* **87**, 688 (1952).
3. G. Salzman, *Phys. Rev.* **99**, 973 (1955).
4. D.R. Yennie *et al.*, *Rev. Mod. Phys.* **29**, 144 (1957).
5. F.J. Ernst *et al.*, *Phys. Rev.* **119**, 1105 (1960).
6. A.F. Sill *et al.*, *Phys. Rev. D* **48**, 29 (1993).
7. R.C. Walker *et al.*, *Phys. Rev. D* **49**, 5671 (1994).
8. L. Andivahis *et al.*, *Phys. Rev. D* **50**, 5491 (1994).
9. V. Punjabi, these proceedings.
10. M. Conversi *et al.*, *Nuovo Cimento* **XL**, 690 (1965).
11. D.L. Hartill *et al.*, *Phys. Rev.* **184**, 1415 (1969).
12. M. Castellano *et al.*, *Nuovo Cimento A* **14**, 1 (1973).
13. G. Bassompierre *et al.*, *Phys. Lett. B* **68**, 477 (1977).
14. B. Delcourt *et al.*, *Phys. Lett. B* **86**, 395 (1979).
15. D. Bisello *et al.*, *Nucl. Phys. B* **224**, 379 (1983).
16. D. Bisello *et al.*, *Z. Phys. C* **48**, 23 (1990).
17. G. Bardin *et al.*, *Nucl. Phys. B* **411**, 3 (1994).
18. A. Antonelli *et al.*, *Phys. Lett. B* **334**, 431 (1994).
19. C. Baglin *et al.*, *Phys. Lett. B* **163**, 400 (1985).
20. T.A. Armstrong *et al.*, *Phys. Rev. Lett.* **70**, 1212 (1993).
21. A. Zichichi *et al.*, *Nuovo Cimento* **XXIV**, 170 (1962).
22. D. Allspach *et al.*, *Nucl. Instrum. Methods A* **410**, 195 (1998).
23. S. Trokenheim *et al.*, *Nucl. Instrum. Methods A* **355**, 308 (1995).
24. L. Bartoszek *et al.*, *Nucl. Instrum. Methods A* **301**, 47 (1991).
25. S. Bagnasco *et al.*, *Nucl. Instrum. Methods A* **424**, 304 (1999).
26. S. Bagnasco *et al.*, *Nucl. Instrum. Methods A* **409**, 75 (1998).
27. M. Ambrogiani *et al.*, *Nucl. Instrum. Methods A* **419**, 632 (1998).
28. G. Oleynik *et al.*, *IEEE Trans. Nucl. Sci.* **41**, 45 (1994).
29. G.J. Feldman and R.D. Cousins, *Phys. Rev. D* **57**, 3873 (1998).
30. G. Lepage and S. Brodsky, *Phys. Rev. Lett.* **43**, 545 (1979).
31. G. Lepage and S. Brodsky, *Phys. Rev. D* **22**, 2157 (1980).
32. P. Kroll *et al.*, *Phys. Lett. B* **316**, 546 (1993).
33. T. Gousset and B. Pire, *Phys. Rev. D* **51**, 15 (1995).